A SHAPING TECHNIQUE FOR AIR-BORNE SCANNING REFLECTOR ANTENNA

Xiaoming Liu[1, 2, *], Junsheng Yu[1], Xiaodong Chen[2], Yuan Yao[1], Cheng Yang[1], and Zejiang Lu[1]

[1]School of Electronic Engineering, Beijing University of Posts and Telecommunications, Beijing 100876, China,

[2]School of Electronic Engineering and Computer Science, Queen Mary University of London, London E1 4NS, UK

Abstract—With the renewed application of millimeter technology in remote sensing, radio astronomy, and meteorological satellite, millimeter wave antennas of electrically large aperture are frequently deployed. Shaping techniques are accordingly developed to meet different requirements. In this paper, a shaping technique for the scanning reflector antenna system of a remote sensing spacecraft is presented. The shaping technique is based on Fourier optical theory to control the maximal radiating direction of the antenna system. To implement such functionality, a new shaping technique of the sub-reflector has been developed. In addition, rotation of the shaped sub-reflector can achieve scanning purpose with identical footprints in all scanning angles. Case studies have been performed to verify the shaping technique.

1. INTRODUCTION

Millimeter wave techniques have been widely employed in remote sensing, radio astronomy, meteorological satellite, and so forth. A number of missions have been deployed with millimeter wave system. For instance, the UK Meteorological Office funded AMSU-B [1], Planck and Herschel spacecrafts launched in 2009 [2], millimeter and sub-millimeter wave acquisitions for stratosphere/troposphere exchange research (MASTER) [3], Chinese Feng-Yun series of meteorological satellites [4] have all deployed with millimeter wave sounding systems.

To detect the signal from target area, the scanning mechanisms vary with different missions. AMSU-B equipped with a downward-looking earth remote sensing radiometer can repetitively do cross-track scanning of the boresight of the radiometer's antenna [1]. Planck is rotating the whole spacecraft to map the cosmic background radiation. Herschel uses a nodding/morphing sub-reflector providing limited image scanning. Since using gross movement can change the observation section, by combination of moving sub-reflector and gross movement, larger area scanning can be achieved.

Nevertheless, the aforementioned scanning mechanisms are mainly achieved through mechanical movement of either the antenna or the spacecraft or both, without imposing any requirement on antenna design. Mechanical scanning brings a problem of stability of the spacecraft. The movement of the whole antenna system produces momentum that needs to be balanced using counter-momentum components, which complicates the design and operation of the whole system. If the momentum can be reduced by introducing proper antenna design technique, the stringent demand on spacecraft can be relaxed. To meet this requirement, shaping techniques can be brought in. The shaping of reflector is to numerically define the surface of reflectors by conforming to specific rules. The shaping technique has a long history, dating back to early 1960s. Later on, a number of shaping techniques have been developed to meet different applications [5–15]. Collins [5] investigated the shaping technique to maximize the aperture efficiency of Cassegrainian Antennas. Lee et al. [6] used geometrical optics to design offset-fed dual-reflector antennas, where satisfactory sidelobes and aperture efficiency were obtained. Kildal [8] developed a dynamic ray tracing technique to analyze multi-reflector antennas of numerically specified reflectors. Bucci et al. [11] proposed a new synthesis algorithm for shaped, double-reflector antennas with complex array feed to improve the efficiency of synthesis techniques without missing the required accuracy. Chou [13] developed an approach of a shaped reflector antenna synthesis using a steepest decent method. Gonzalez-Valdes et al. [15] proposed a physical optics based approach to compensate the surface distortion due to thermal and gravitational effects.

In this work, we present a different shaping technique to achieve scanning purpose for the prototype of a remote sensing spacecraft. The mission requires a conventional Cassegrain antenna structure, with the main reflector a circular symmetric surface, while the sub-reflector a shaped one. Differently to conventional Cassegrain antenna, the output beam is demanded slightly tilted off the axis of the main dish. By rotating the sub-reflector, the antenna can form a series of footprints

on the Earth of identical radiation pattern. In addition, rotating the sub-reflector can reduce the gross momentum compared to rotating the whole antenna system. The aforementioned shaping techniques do not fit these requirements completely. For instance, the method presented by Collins [5] did not consider the functionality of scanning; Lee's method [6] is suitable for offset structure, which is not employed in the mission; Bucci's [11] method is suitable for cases where feed array is utilized. In this regards, a new shaping scheme has to be developed. The following parts of this paper are organized as follows: Section 2 discusses the fundamental theory; Section 3 describes the procedures of the shaping technique; Section 4 presents representative case studies; Conclusions are in Section 5.

2. FUNDAMENTAL THEORY OF SHAPED ANTENNA

2.1. General Consideration

The function of a shaped reflector antenna is transforming the amplitude and/or phase distribution of incident fields to desired ones. Whichever the shaping technique is, two general rules have to be observed rigorously. One is the conservation rule of energy, and the other is equal optical path. The formal and the later rules dedicate the amplitude and the phase distribution, respectively.

In general, the farfield of an antenna is the Fourier transform of its near field [16, 17]. Mathematically, the near field is a spatial function, which can be decomposed to a series of plane wave propagating in different directions

$$F\left(k_x, k_y\right) = \int\limits_{-\infty}^{+\infty} \int\limits_{-\infty}^{+\infty} E\left(x, y\right) \cdot e^{j(k_x x + k_y y)} dx dy, \tag{1}$$

where k_x, k_y are wavenumbers in the x and y directions. The components of each individual direction can be referred to as angular spectra. The farfield is therefore the superposition of the plane waves in a certain distance sufficiently far from the near field. As shown in [17], the farfield can be asymptotically expressed as

$$E\left(R, \theta, \varphi\right) = \frac{jk_0 \cos\theta e^{-jk_0 R}}{R} F\left(k_x, k_y\right). \tag{2}$$

And k_x, k_y can be written as

$$\begin{cases} k_x = k_0 \sin\theta \cos\varphi \\ k_y = k_0 \sin\theta \sin\varphi \end{cases} \tag{3}$$

where k_0 is the wavenumber in free space. It is clearly seen that the magnitude of the farfield is largely determined by its plane wave spectra. By making use of this principle, one can design antennas of specific requirements. If a certain direction of the angular spectra is larger enough than other directions, the maximal gain is most likely to appear in this direction.

2.2. Fourier Transform of Near Field

Considering an aperture, over which the amplitude of the electric field is uniformly distributed and the phase is a linear function of y, as shown in Figure 1. Mathematically, the field distribution can be expressed as

$$E(x, y) = e^{jk_{0y}y}, \quad -T < x, y < T, \tag{4}$$

where T defines the boundary of the aperture, and k_{0y} defines an equal phase plane. The angular spectra can be calculated by applying Fourier transform

$$F(k_x, k_y) = \int_{-T}^{+T} \int_{-T}^{+T} E(x, y) \cdot e^{j(k_x x + k_y y)} dx dy$$
$$= \frac{2 \sin(T \cdot k_x)}{k_x} \cdot \frac{2 \sin[T \cdot (k_{0y} + k_y)]}{k_{0y} + k_y}. \tag{5}$$

The first and second terms of Equation (5) are sinc functions having their maximal value when the variable is zero. Therefore, the maximal spectrum finds to be

$$\vec{k} = (k_x, k_y, k_z) = \left(0, -k_{0y}, \sqrt{k_0^2 - k_{0y}^2}\right), \tag{6}$$

Amp[$E(x,y)$]=1, -$T<x,y<T$ Arg[$E(x,y)$]=$k_{0y}y$, -$T<x,y<T$

(a)   (b)
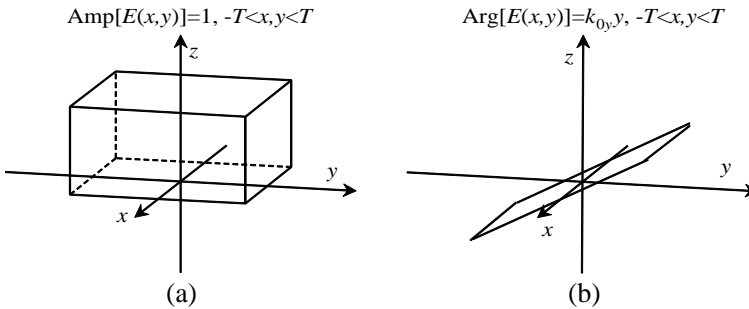
Figure 1. A field distribution. (a) Unifrom amplitude distribution. (b) Linear phase distribution.

where, k_0 is the wavenumber in free space. The corresponding maximal radiation direction (φ, θ) can be calculated using Equation (3), with $\varphi = 90°$, $\theta = -\arcsin(k_{0y}/k_0)$. It can be seen from Equations (4) and (6) that the maximal radiation direction is determined by the equal phase plane. To investigate the effect of the aperture size on the radiation pattern, the spectral components in the y-axis are plotted against T. As shown in Figure 2, when T increases, the magnitude of the spectra at $k_y = k_{0y}$ becomes increasing dominant. If the aperture is infinite large, $k_y = k_{0y}$ is the only spectral component, and subsequently, the farfield becomes a plane wave.
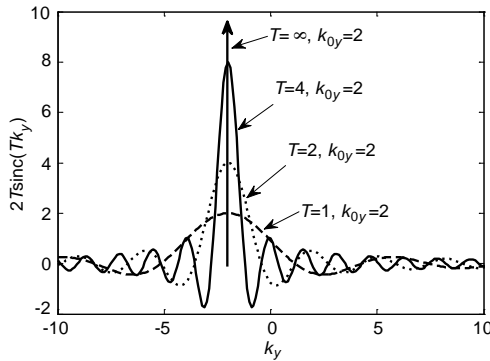
Figure 2. Angular spectra of different T.

For a circular aperture, i.e., $\sqrt{x^2 + y^2} < T$, it can be proved that the peak radiation direction is the same as Equation (6). If the amplitude distribution is a Gaussian type, while the phase is that of Figure 1(b), for example

$$E(x, y) = e^{-\left(ax^2 + by^2\right)} \cdot e^{jk_{0y}y}. \tag{7}$$

Fourier transform yields

$$F(k_x, k_y) = \frac{\pi}{\sqrt{ab}} \cdot \exp\left[-\frac{k_x^2}{4a} - \frac{(k_{0y} + k_y)^2}{4b}\right]. \tag{8}$$

Again, the maximal radiation direction is that given by Equation (6). Gaussian type distribution is a good approximation in many systems, such as the output field of a Cassegrain antenna.

These two examples are of practical importance in the design of antenna system. To generate a reflector antenna with desired radiation direction, a possibility is to make the equal phase plane perpendicular to the desired radiation direction.

3. SHAPING PROCEDURES

The scanning antenna system is designed to rotate the sub-reflector and subsequently forming a scanning loop, as shown in Figure 3. Each loop consists of a few identical footprints. The main reflector is a circular symmetric surface about the boresight direction of the antenna, while the output rays are at an angle of θ_0 to the boresight direction. The shaping technique is to numerically define the sub-reflector so as to fulfill such functionalities. The diagram of synthesis of the scanning antenna system is schematically illustrated in Figure 3. To implement such a shaping technique, the main dish has to be known as a prior. Also the optical centers of the sub-reflector and the aperture, and the location of the feed have to be defined before starting the shaping procedures. The synthesis procedures are as follows.
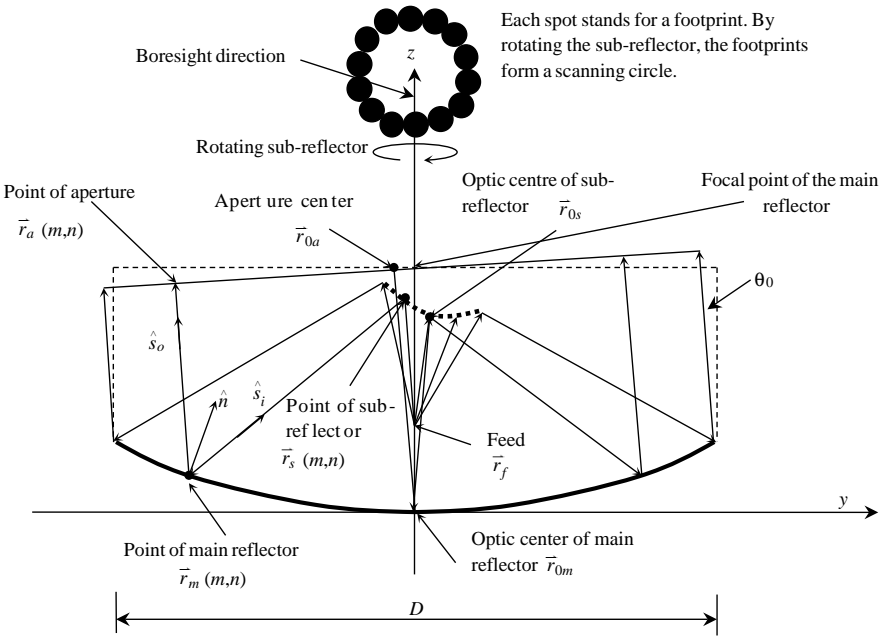
Figure 3. The scanning scheme of the antenna system. The main reflector has a symmetry structure, the sub-reflector is a shaped dish. By rotating the sub-reflector, the scanning can form a loop with identical footprints. The equal phase plane is perpendicular to the output rays.

Step 1: Determine the surface profile of the main reflector

$$z = \frac{x^2 + y^2}{4f},$$ (9)

where f is the focal length of the parabolic, or the main reflector. And z-direction is assumed to be the boresight direction of the antenna. It has to be mentioned that, the surface of the main reflector does not necessarily need to be a paraboloid. Any circularly symmetric surface can do in this method. The only difference is the normal vector of the surface;

Step 2: Determine the optical centers of the main reflector, sub-reflector, and the aperture, $\vec{r}_{0m}$, $\vec{r}_{0s}$, $\vec{r}_{0a}$, and the position of the feed $\vec{r}_f$. The optical center of the main reflector is the geometrical center of the surface. The optical center of the aperture is defined as

$$\vec{r}_{0a} = f \cdot (-\sin\theta_0, 0, \cos\theta_0).$$ (10)

This can ensure the reflected ray from the optical center of the main reflector going through the optical center of the aperture meanwhile at an angle of θ_0 to the boresight direction of the antenna. The optical center of the sub-reflector is chosen as

$$\vec{r}_{0s} = af \cdot (\sin\theta_0, 0, \cos\theta_0),$$ (11)

with $0.5 < a < 1$. In Equation (11), a is used to define the optical center of the sub-reflector. The reason for choosing this range for a is that (1) for a conventional Cassegrain antenna, the focus of the hyperboloidal reflector has to be coincide with that of the paraboloidal reflector, which requires that the vertex of the hyperboloidal reflector lays between the two foci of the hyperboloidal reflector ($a < 1$); and (2) The vertexes of the two branch of the hyperboloidal reflector have to be separate with each other ($0.5 < a$);

Step 3: Calculate the optical path from the feed to the aperture center

$$T = \left|\vec{r}_{0s} - \vec{r}_f\right| + \left|\vec{r}_{0m} - \vec{r}_{0s}\right| + \left|\vec{r}_{0a} - \vec{r}_{0s}\right|.$$ (12)

Step 4: Choose a set of points on the surface of the main reflector, we use parabolodial surface as an example

$$\vec{r}_m(m, n) = (x_m, y_m, \frac{x_m^2 + y_m^2}{4f}),$$ (13)

and calculate the unit normal vector at this point. For a parabolodial surface

$$\hat{n} = \frac{(-\frac{x_m}{2f}, -\frac{y_m}{2f}, 1)}{\sqrt{\frac{x_m^2 + y_m^2}{4f^2} + 1}}.$$ (14)

Step 5: Determine the point on the aperture

$$\vec{r}_a(m, n) = \vec{r}_m(m, n) + s\hat{s}_o, \tag{15}$$

where $\hat{s}_o$ is the direction of output rays

$$\hat{s}_o = [-\sin(\theta_0), 0, \cos(\theta_0)], \tag{16}$$

where, θ_0 is the polar angle of the output rays, i.e., the desired radiation direction. The aperture plane can be represented using

$$\hat{s}_o \cdot [\vec{r}_a(m, n) - \vec{r}_{0a}] = 0. \tag{17}$$

This immediately gives s as

$$s = [\vec{r}_{0a} - \vec{r}_m(m, n)] \cdot \hat{s}_o. \tag{18}$$

Step 6: Calculate the input ray using Snell's law

$$\hat{s}_i = 2(\hat{s}_o \cdot \hat{n})\hat{n} - \hat{s}_o. \tag{19}$$

Step 7: Represent the point on the sub-reflector using

$$\vec{r}_s(m, n) = \vec{r}_m(m, n) + t\hat{s}_i, \tag{20}$$

where t is the distance between the point on the main reflector and the corresponding point on the sub-reflector. So, t is the only unknown needed to determine the point on the sub-reflector.

Step 8: The equal path principle dedicated that each ray from the feed to the aperture plane must has the same optical path length, which results in an equal phase plane on the aperture. Using the equal path principle, it holds that

$$\left|\vec{r}_a(m, n) - \vec{r}_m(m, n)\right| + t + \left|\vec{r}_s(m, n) - \vec{r}_f\right| = T. \tag{21}$$

It can be written as

$$\left|\vec{r}_a(m, n) - \vec{r}_m(m, n)\right| + t + \left|\vec{r}_m(m, n) + t\hat{s}_i - \vec{r}_f\right| = T. \tag{22}$$

After mathematical manipulation, t finds to be

$$t = \frac{\left[T - \left|\vec{r}_a(m, n) - \vec{r}_m(m, n)\right|\right]^2 - \left|\vec{r}_m(m, n) - \vec{r}_f\right|^2}{2\hat{s}_i \cdot \left[\vec{r}_m(m, n) - \vec{r}_f\right] + T - \left|\vec{r}_a(m, n) - \vec{r}_m(m, n)\right|}. \tag{23}$$

Inserting Equation (23) to Equation (20), the point on the sub-reflector can be found.

Step 9: Since the surface of the sub-reflector is to be numerically defined using discrete points, and we always start the procedure from the main reflector, the main reflector has to be represented using discrete points. Here we use polar-grid discrete points

$$\vec{r}_m(m, n) = (m\Delta\rho, n\Delta\phi), \tag{24}$$

where n and $\Delta\phi$ can be functions of m. And $\Delta\rho$ is the maximal distance between two neighboring points. Therefore, the Cartesian coordinates can be written as

$$x_m(m, n) = m\Delta\rho\cos(n\Delta\phi), \quad y_m(m, n) = m\Delta\rho\sin(n\Delta\phi) \quad (25)$$

where, $\Delta\phi$ and n can be determined by

$$\begin{cases} m\Delta\rho\Delta\phi \leq \Delta\rho \Rightarrow \Delta\phi \leq \frac{1}{m} \\ n \geq \frac{2\pi}{\Delta\phi} = 2\pi m \end{cases}. \quad (26)$$

By circulating m and n, and repeating Step-4 to Step-8, the shaped sub-reflector can be defined.

4. CASE STUDY

To verify this shaping technique, we have simulated two models using the commercial software GRASP 10.0, which is based on physical optical theory.

CASE-1: The main dish is a paraboloidal reflector. The main parameters are as follows:

(1) The focal length of the main reflector $f = 0.8\,\text{m}$. The aperture size of the main reflector is $D = 2\,\text{m}$;

(2) The scanning angle $\theta_0 = 1.6°$;

(3) The optical centers of the main reflector, sub-reflector, the aperture, and the location of the feed are

$$\begin{cases} \vec{r}_{0m} = (0, 0, 0) \\ \vec{r}_{0s} = 0.65[\sin(\theta_0), 0, \cos(\theta_0)] \\ \vec{r}_{0a} = 0.8[-\sin(\theta_0), 0, \cos(\theta_0)] \\ \vec{r}_f = (0, 0, 0) \end{cases}. \quad (27)$$

By inputting these parameters to the procedures in Section 3, the shaped dish can be defined.

(4) The feed is a conventional Gaussian-type distribution with edge taper of $-14\,\text{dB}$ at $13°$. It has to be mentioned that the edge taper is choosing to achieve optimized aperture efficiency as explained in [18];

(5) Simulation frequencies are 54, and 119 GHz.

The diagram of the whole system is shown in Figure 4. The shaped sub-reflector is not a symmetrical structure as that in a conventional front-feed Cassegrain antenna. In this case, the sub-reflector extends from -156.8 to $260.5\,\text{mm}$ in the Y-axis direction, while from -211.0 to $211.0\,\text{mm}$ in the X-axis direction. The reason for that the sub-reflector
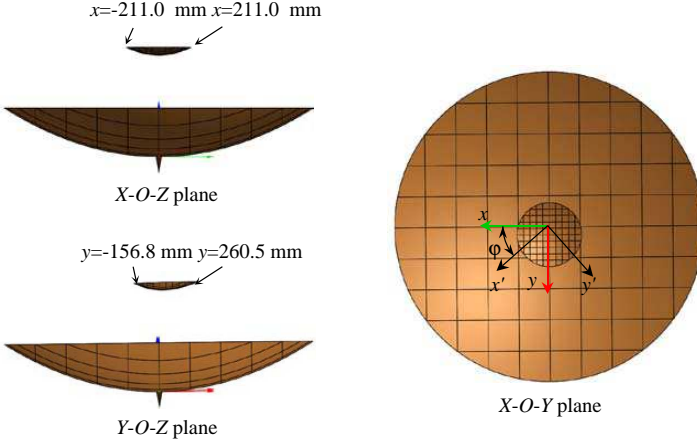
Figure 4. The diagram of the shaped reflector system rendered in commercial software GRASP.

is not symmetrical in the Y-axis direction is that, in this design, the output direction is designed to ($\varphi = 90°$, $\theta = -1.6°$), which makes the sub-reflector looks tilting towards the positive-Y axis.

The near fields of the main reflector are plotted in Figure 4. It is clearly seen that the sub-reflector blocks the output waves. The edge of the sub-reflector produces a certain degree of diffraction. In the blockage region, the amplitude is very small, averagely -20 dB taper off. However, the amplitude is not our main concern. It is shown in Figure 5(b) that except the blockage region, the phase slope is 1.96 degree/mm (the results of 54 GHz), which is consistent with the theoretical prediction by the optical path difference

$$slope = \frac{\sin \theta_0}{\lambda} \cdot 360 \ (°/\text{mm}),\tag{28}$$

where, wavelength is in mm, and θ_0 is the pointing angle as shown in Figure 3. It has to be mentioned that the phase is only constrained to the range of $(-180°, 180°)$. Therefore a serrated profile is observed. It is consequently more reasonable to observe the slope of the phase. Regarding the slope of the phase, two points have to be noted. In to (1) in the simulation, the near field plane is perpendicular to the z-axis in Figure 3; (2) the equal-phase plane is at an angle of θ_0 to the near field plane. In consequence, the optical path difference between two arbitrary points separated by unit distance in the y direction on the near field plane is $\sin \theta_0$, and in electrical length $\sin \theta_0/\lambda$. Therefore, the slope for the phase can be calculated by Equation (28).
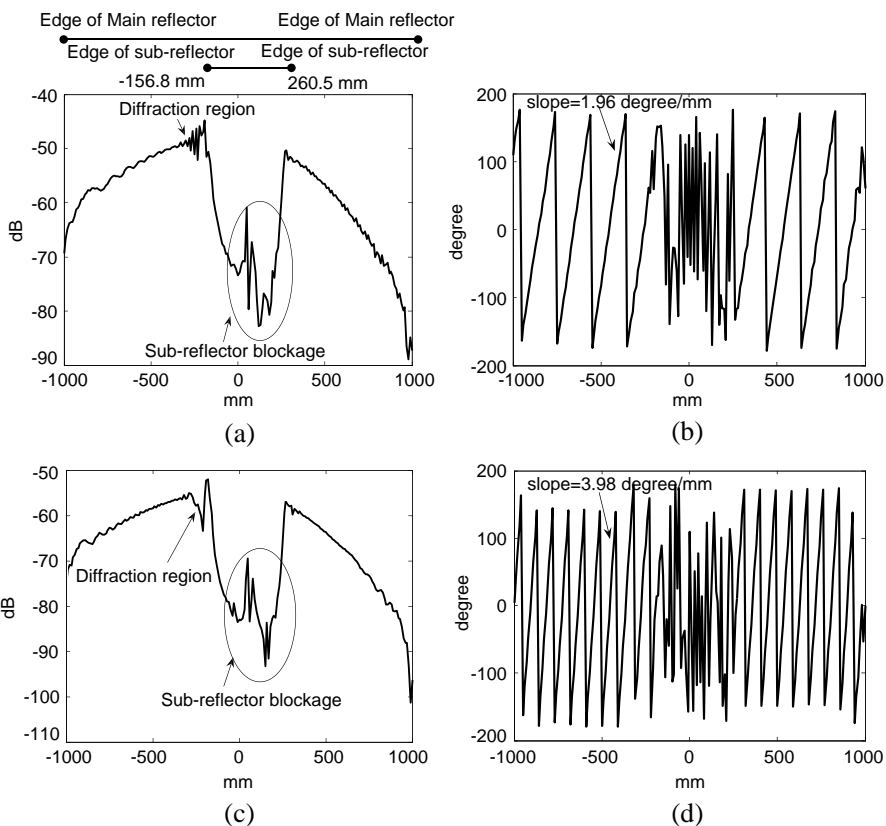
Figure 5. The near fields of the antenna. (a) 54 GHz amplitude. (b) 54 GHz phase. (c) 119 GHz amplitude. (d) 119 GHz phase.

According to the theory of Section 2, the simulation results shown in Figure 5 shall imply that the maximal gain direction is in the direction of $(\varphi = 90°, \theta = -1.6°)$. Examining the farfield, as shown in Figure 6, it is seen that the maximal radiation pattern in $\theta = -1.6°$, which is in agreement of the theoretical prediction. It has to be mentioned that, the farfield is referenced to the global system. We use slightly different definition of the spherical system. Azimuthal angle φ is restricted to $[0, 180)$, while polar angle θ is extended to $[-90, 90]$.

Further to this, it is seen the spillover range from the feed is in the range of -10 to -16 dB, centered at -13 degree. The signal of spillover is more than 60 dB below the main lobe, indicating that the stray rays shall make very small difference to the performance of the antenna. Besides, the 3 dB beam is a symmetrical spot, not shown
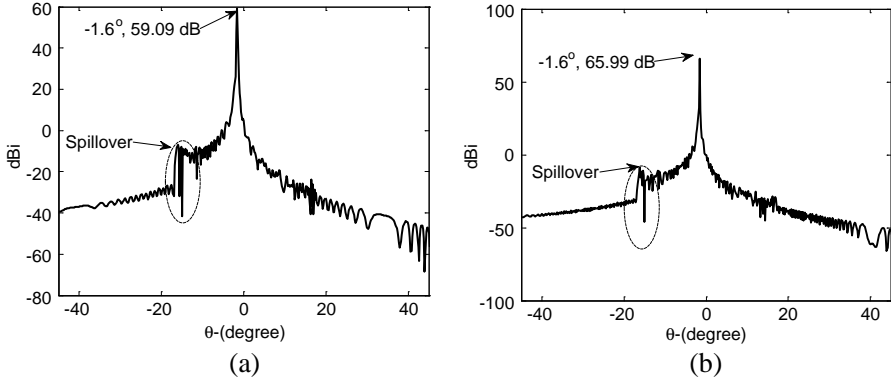
Figure 6. The gain pattern of the antenna system of parabloidal main reflector. (a) 54 GHz. (b) 119 GHz.

in the results. By rotating the sub-reflector, a scanning loop can be formulated with identical footprints. Identical footprint is always preferred for a scanning scheme, since that each scanning pixel has the identical imaging quality. The main beam efficiency (main beam is defined as 2.5 times 3 dB beamwidth) is calculated to be around 75.0%, which is a typical value for a front-feed Cassegrain antenna.

For 119 GHz, the same observation can be made from the results. The slopes of the phase also agree with the prediction. The maximal radiation direction is $(\varphi = 90°, \theta = -1.6°)$. In addition, it is seen that the diffraction looks less prominent than that of 54 GHz.

To further verify this shaping algorithm, a spheroidal main reflector has been modeled. As is mentioned, any symmetrical surface can be used for the design of such a canning antenna system, while not affecting the procedures of shaping. The only difference that needs to be stressed to to be stressed is the normal unit vector of the main reflector.

CASE-2: The main dish is a spheroidal reflector. The main parameters are as follows:

(1) The radius of the spheroidal reflector $R = 2.4$ m. The aperture size of the main reflector is $D = 2$ m;

(2) The optical centers of the main reflector, sub-reflector, the aperture, and the location of the feed are

$$
\begin{cases}
\vec{r}_{0m} = (0,0,0) \\
\vec{r}_{0s} = 0.8\left[\sin\left(\theta_0\right),0,\cos\left(\theta_0\right)\right] \\
\vec{r}_{0a} = 1.2\left[-\sin\left(\theta_0\right),0,\cos\left(\theta_0\right)\right] \\
\vec{r}_f = (0,0,0)
\end{cases}
. \tag{29}
$$

Other parameters are the same as that in Case-1. In this case, only the farfields are presented, as shown in Figure 7. It is also seen that the gain of farfields peaks in the direction of ($\varphi = 90°$, $\theta = -1.6°$). Again, it has symmetrical 3 dB beam spot (not shown). However, the spillover of this design is much more prominent than that of CASE-1. The reason may be attributed to the fact that in CASE-2, a smaller sub-reflector has been synthesized, which may also explain the peak gain is slightly smaller than that of CASE-1.
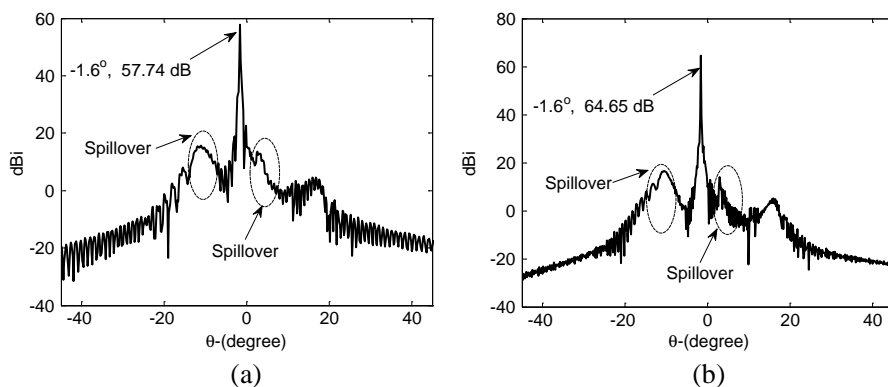
Figure 7. The gain pattern of the antenna system of spherical main reflector. (a) 54 GHz. (b) 119 GHz.

It has to be mentioned that in the preliminary design of the scanning antenna, offset structure was proposed due to its higher efficiency. However, offset Cassegrain antenna does not produce identical footprints. Also, the scanning of an offset structure is more complicated than a front-feed one. In the future work, efforts are being taken to reduce spillover and increase main beam efficiency.

Since the main dish is a symmetrical paraboloidal structure, the rotation of the sub-reflector about z-axis (see Figure 3) does not actually modify the radiation pattern, but only change the radiation direction. As shown in Figure 4, when the sub-reflector rotates about Z-axis by an angle of φ, the whole system acts like rotating about Z-axis by an angle of φ due to the symmetrical nature of the main reflector. Therefore, the radiation pattern rotates by an angle of φ about Z-axis. Indeed, in the simulation, we have observed this phenomenon. Since the radiation pattern are identical (By identical, it is meant, if one rotates the pattern by an angle of φ, the two radiation patterns coincide with each other), the results are not shown. This phenomenon can also be deduced from Equations (4) and (5). The rotation of the sub-reflector in essence is changing the orientation of

the equal-phase plane by an angle of φ. Mathematically, the near field can be written as

$$E\left(x, y\right) = e^{jk_{0y}(x\cos\varphi+y\sin\varphi)}, \quad -T < x, y < T, \tag{30}$$

The resultant spectra read

$$F\left(k_x, k_y\right) = \int\limits_{-T}^{+T}\int\limits_{-T}^{+T} E\left(x, y\right) \cdot e^{j(k_x x+k_y y)} dxdy$$

$$= \frac{2\sin\left[T \cdot (k_{0y}\cos\varphi+k_x)\right]}{k_{0y}\cos\varphi + k_x} \cdot \frac{2\sin\left[T \cdot (k_{0y}\sin\varphi+k_y)\right]}{k_{0y}\sin\varphi + k_y}. \tag{31}$$

And the maximal spectrum moves to

$$\vec{k} = (k_x, k_y, k_z) = \left(-k_{0y}\cos\varphi, -k_{0y}\sin\varphi, \sqrt{k_0^2 - k_{0y}^2}\,\right). \tag{32}$$

From Equation (3), it can be seen that $k_{0y} = -k_0\sin\theta$, which means, azimuthal angle φ does not change the maximal radiation polar angle θ. The rotation of the sub-reflector only rotates the radiation pattern by the same angle of φ in the azimuthal angle direction.

5. CONCLUSION

A shaping technique based on Fourier Optics has been described in this paper. To design the required maximal radiation direction, the equal-phase plane has to be perpendicular the maximal radiation direction angle. The simulated results of farfields indicated that the shaping of sub-reflector using this shaping technical could manipulate the maximal radiation direction, as well as achieving scanning purpose with identical footprints in all scanning angles. Future work will focus on reducing spillover and increasing main beam efficiency.

ACKNOWLEDGMENT

REFERENCES

1. Martin, R. J. and D. H. Martin, "Quasi-optical antennas for radiometric remote sensing," *Electronics & Communication Engineering Journal*, Vol. 8, 37–48, 1996.

2. Doyle, D., G. Pilbratt, and J. Tauber, "The herschel and planck space telescopes," *Proceedings of the IEEE*, Vol. 97, 1–9, 2009.

3. Jørgensen, R., G. Padovan, P. de Maagt, and L. Costes, "A 5-frequency millimeter wave antenna for a spaceborne limb sounding instrument," *IEEE Trans. Antennas Propagat.*, Vol. 49, 703–714, 2001.

4. Jin, Y., N. Lu, and M. Lin, "Advancement of Chinese meteorological Feng-Yun (FY) and oceanic Hai-Yang (HY) satellite remote sensing," *Proceedings of the IEEE*, Vol. 98, 844–861, 2010.

5. Collins, G. W., "Shaping of subreflectors in cassegrainian antennas for maximal aperture efficiency," *IEEE Trans. Antennas Propagat.*, Vol. 21, 309–313, 1973.

6. Lee, J. J., L. I. Parad, and R. S. Chu, "A shaped offset-fed dual-reflector antenna," *IEEE Trans. Antennas Propagat.*, Vol. 272, 165–171, 1979.

7. Bergmann, J., R. C. Brown, P. J. B. Clarricoats, and H. Zhou, "Synthesis of shaped-beam reflector antenna patterns," *IEE Proceedings*, Vol. 135, 48–53, 1988.

8. Kildal, P., "Analysis of numerically specified multireflector antennas by kinematic and dynamic ray tracing," *IEEE Trans. Antennas Propagat.*, Vol. 38, 1600–1606, 1991.

9. Descardeci, J. R. and C. G. Parini, "Trireflector compact antenna test range," *IEE Proceedings*, Vol. 144, 305–310, 1997.

10. Hoferer, R. A. and Y. Rahmat-Samii, "Subreflector shaping for antenna distortion compensation: An efficient Fourier-Jacobi expansion with GO/PO analysis," *IEEE Trans. Antennas Propagat.*, Vol. 50, 1676–1687, 2002.

11. Bucci, O. M., A. Capozzoli, and G. D'Elia, "An effective power synthesis technique for shaped, double-reflector multifeed antennas," *Progress In Electromagnetics Research*, Vol. 39, 93–123, 2003.

12. Liu, S. D., S. F. Liu, Y. C. Jiao, and F. S. Zhang, "Shaping design of side-fed offset cassegrain refector antennas," *PIERS Proceedings*, 165–169, Hangzhou, China, Mar. 24–28, 2008.

13. Chou, H.-H., "Fast SDM for shaped reflector antenna synthesis via patch decompositions in PO integrals," *Progress In Electromagnetics Research*, Vol. 92, 361–375, 2009.

14. Eom, S.-Y., Y.-B. Jung, S. A. Ganin, and A. V. Shishlov, "A cylindrical shaped-reflector antenna with a linear feed array for shaping complex beam patterns," *Progress In Electromagnetics*

Research, Vol. 119, 477–495, 2011.

15. Gonzalez-Valdes, B., J. Martinez-Lorenzo, C. Rappaport, and A. García Pino, "A new physical optics based approach to sub-reflector shaping for reflector antenna distortion compensation," *IEEE Trans. Antennas Propagat.*, Vol. 67, 467–472, 2013.

16. Balanis, C. A., *Antenna Theory Analysis and Design*, Chapter 12, John Wiley & Sons, New Jersey, 2005.

17. Johnson, R. C., H. A. Ecker, and J. S. Hollis, "Determination of far-field antenna patterns from near-field measurements," *Proceedings of the IEEE*, Vol. 61, 1668–1694, 1973.

18. Kindal, P.-S., "The effects of sub-reflector diffraction of aperture efficiency of conventional Cassegrain antenna-an analytical approach," *IEEE Trans. Antennas Propagat.*, Vol. 31, 903–909, 1983.